



HAL
open science

Shear wave modes in an equilateral triangular prismatic bar

Omar Asfar, Bruno Morvan

► **To cite this version:**

Omar Asfar, Bruno Morvan. Shear wave modes in an equilateral triangular prismatic bar. Journal of the Acoustical Society of America, 2023, 154 (2), pp.968-978. 10.1121/10.0020654 . hal-04187085

HAL Id: hal-04187085

<https://normandie-univ.hal.science/hal-04187085>

Submitted on 30 May 2024

HAL is a multi-disciplinary open access archive for the deposit and dissemination of scientific research documents, whether they are published or not. The documents may come from teaching and research institutions in France or abroad, or from public or private research centers.

L'archive ouverte pluridisciplinaire **HAL**, est destinée au dépôt et à la diffusion de documents scientifiques de niveau recherche, publiés ou non, émanant des établissements d'enseignement et de recherche français ou étrangers, des laboratoires publics ou privés.



Distributed under a Creative Commons Attribution 4.0 International License

AUGUST 15 2023

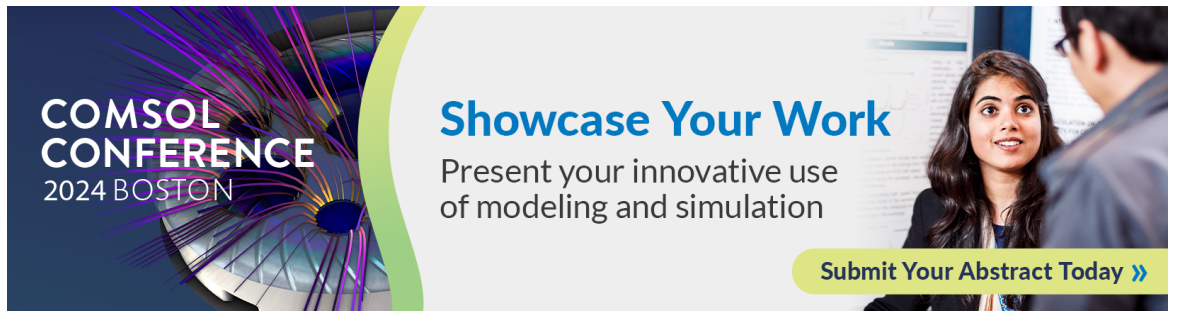
Shear wave modes in an equilateral triangular prismatic bar

Omar Asfar; Bruno Morvan 



J. Acoust. Soc. Am. 154, 968–978 (2023)

<https://doi.org/10.1121/10.0020654>



COMSOL CONFERENCE
2024 BOSTON

Showcase Your Work

Present your innovative use of modeling and simulation

[Submit Your Abstract Today >>](#)

Shear wave modes in an equilateral triangular prismatic bar

Omar Asfar^{1,a)} and Bruno Morvan² 

¹Department of Electrical Engineering, Jordan University of Science and Technology, Irbid 22110, Jordan

²Laboratoire Ondes et Milieux Complexes, Unité Mixte de Recherche, Centre National de la Recherche Scientifique 6294, Université du Havre, 75 Rue Bellot CS 80540, 76058 Le Havre Cedex, France

ABSTRACT:

Shear wave excitation of an equilateral triangular solid bar shows the existence of horizontally polarized (SH) and vertically polarized (SV) shear waves. The SH wave modes are Lamé solutions of the Neumann problem for displacement and Dirichlet problem for stress in the equilateral triangle. It is shown that Lamé's solutions are obtained from superposition of three equal plane waves and their reflections. The Neumann SH modes have cutoff wavenumber $4m\pi/(3a)$, where $m = 1, 2, 3, \dots$, a being the side length of triangular cross section. The first Dirichlet SH mode has a higher cutoff wavenumber $4\pi\sqrt{7}/(3a)$. The SV modes are related to the 30° – 60° – 90° and 30° – 120° – 30° sub triangles. Their cutoff wavenumbers lie between those of the first ($m = 1$) and second ($m = 2$) Neumann SH modes. The standing wave condition in each sub triangle is related to three unequal plane waves which decompose via symmetrical component analysis into two different sets of equal plane waves. A nonlinear product solution based on the new plane wave set leads to modal SV wave solutions. Dispersion curves calculated using COMSOL confirm the correct cutoff wavenumbers of both SH and SV waves. Normal displacement mode shapes are calculated analytically and verified experimentally using laser vibrometer with good agreement for all modes.

© 2023 Author(s). All article content, except where otherwise noted, is licensed under a Creative Commons Attribution (CC BY) license (<http://creativecommons.org/licenses/by/4.0/>). <https://doi.org/10.1121/10.0020654>

(Received 2 May 2023; revised 25 July 2023; accepted 27 July 2023; published online 15 August 2023)

[Editor: Michel Destrade]

Pages: 968–978

I. INTRODUCTION

This work is part of a program aimed at developing a guided ultrasonic wave inspection technique for nondestructive testing of seam-welded pipes. Based on various studies of weld structure,¹ the weld cross section is made up of three distinct regions: the fusion zone, the heat-affected zone, and the base metal zone. Neutron diffraction studies² have shown that the residual stress in the weld varies with depth in a somewhat finitely periodic manner. This can also be observed by performing surface micro-hardness tests. As the weld structure is very complicated, one can assume the shape of a V-weld to have an equilateral triangular cross section with a number of layers from core to surface in order to develop a simple analytical model for wave propagation. This layered structure is reminiscent of the structure of an optical fiber which supports a guided light wave as a result of the small difference between the indexes of refraction of core and cladding.³ This suggests that a weld will similarly cause an acoustic wave to be guided in view of the different material properties of the three zones. This view is supported by the experimental and finite-element simulation work of Fan⁴ and Fan and Lowe⁵ showing that a shear wave was localized in the weld as a result of the difference in phase velocities between the weld and adjoining metal. As a first step in the investigation, we will identify the guided

shear modes of propagation using a simpler model consisting of a homogeneous equilateral triangular bar subjected to excitation from a shear wave transducer based on a ray technique.

In the field of acoustics, exact solutions of elastic wave propagation in solid bars were limited to circular⁶ and elliptical⁷ cross-sections. Numerical methods were developed for treatment of other cross-sections. Nigro⁸ applied the Ritz method to infinite bars of rectangular cross section. Nagaya⁹ applied the Fourier expansion collocation method to infinite bars of polygonal cross section. Mukdadi *et al.*¹⁰ developed a semianalytical finite element method for the case of layered elastic plates with rectangular cross section. The finite element method was used for guided waves in plates and structural waveguides.^{11–13} Castaings and Lowe¹⁴ developed the SAFE finite-element method for the treatment of guided waves along solid systems of arbitrary cross section coupled to infinite media. The same technique was used to predict energy concentration in large aspect ratio rectangular waveguides at high frequencies by Cegla.¹⁵ Lesage *et al.*¹⁶ generalized Nagaya's method to solid bars with curved boundaries in order to compute dispersion curves for longitudinal and flexural waves. A ray theory of waveguide modes using the geometrical acoustics approximation for wedge structures was formulated by Krylov.¹⁷ Rayleigh¹⁸ gave solutions for the resonant frequencies of an isosceles triangular membrane. Hudson¹⁹ calculated the dispersion curves for elongational and flexural waves in a circular

^{a)}Electronic mail: orasfar@gmail.com

cylindrical bar. In a previous publication,²⁰ we considered the propagation of acoustic waves subject to excitation from a longitudinal wave transducer in an equilateral triangular bar by adapting a plane wave superposition ray technique to the case of acoustics which was verified experimentally as well as by simulation in COMSOL. The nature of the boundary conditions in the case of compressional wave excitation necessitates the presence of a vertically polarized SV shear wave. Assuming SV shear wave incidence, the associated longitudinal wave disappears for a 45° angle of incidence on a free surface. In this paper, we present a plane wave superposition ray technique appropriate for a shear wave transducer for the treatment of shear waves in an equilateral triangular prismatic bar.

An analog of the shear wave transducer in the field of electromagnetics is the differentially fed equilateral triangular patch antenna (ETPA) loaded with shorting posts (Wang *et al.*²¹) The principal resonant modes of the simply fed ETPA are the Lamé solutions of the linear eigenvalue problem in the equilateral triangle.²² New resonances designated as zero modes,²¹ whose frequencies are distinct and do not bear any harmonic relationship to the classical Lamé modes, were observed. The spectrum of new resonances contained a zero one mode with cutoff wavenumber approximately equal to $\pi/\sqrt{3}a$ followed by the first Lamé mode TM_{10} whose cutoff wavenumber is $4\pi/3a$.

In the present work, the same phenomenon of zero modes was detected in simulation using COMSOL and in experiment when the triangular prismatic bar was excited by a shear wave transducer whose model consists of two out-of-phase sources. As will be shown in this paper, the zero modes are a result of standing wave conditions in the 30°–60°–90° and 30°–120°–30° sub triangles within the equilateral triangle which are analysed via the method of symmetrical components well known in the field of electric power systems analysis.^{23,24} A nonlinear product solution for these modes is presented based on a plane wave superposition technique. Interest in how Lamé obtained his solution prompted McCartin^{25,26} to solve Laplace’s equation over the equilateral triangle for both the Dirichlet and Neumann problems by using separation of variables in two coordinates defined over the cross section. The ray technique presented in this paper accurately predicts the cutoff wavenumbers and modal fields in McCartin’s solution. A nonlinear product solution of six standing waves was used by Polya²⁷ to find the fundamental frequency for Dirichlet’s problem in a triangular membrane. His solution was obtained using reflections in the plane from a 30°–60°–90° triangle and predicted a fundamental eigenvalue $4\pi(\sqrt{7}/3a)$ that agrees with the first Dirichlet mode of the equilateral triangle (McCartin²⁵) In this paper, we show that the fundamental cutoff wavenumber of the 30°–60°–90° triangle is $2\pi(\sqrt{7}/3a)$ which is obtained via symmetrical components analysis of the simplest standing wave condition in the half equilateral triangle.

This paper starts with a description of the shear wave transducer used in the experiment and a plane wave

reconstruction model used to derive the cross-sectional mode patterns that it generates as well as a description of the experimental setup in Sec. II. This is followed by application of the model to derive the triangular SH mode shapes that are compared with experiment in Sec. III. The classical Lamé solution of the Dirichlet problem for stress is also presented in Sec. III. The method of symmetrical components is presented in Sec. IV as well as the nonlinear product solution for triangular SV waves and its comparison with experiment. Conclusions follow in Sec. V.

II. SHEAR-WAVE MODEL AND EXPERIMENT

In order to develop a model for shear wave propagation and identify the guided modes, we consider the prismatic waveguide with equilateral triangular cross section that is fitted with a shear-wave transducer positioned at the centroid of the triangular cross section as shown in Fig. 1. In the model, we use two sources 180° out of phase with each other and vibrate transverse to the surface generating a normal displacement function that is antisymmetric with respect to the y axis thereby generating a state of shear in the waveguide. This configuration is used in the experiment and is the basis for the proposed plane wave superposition technique.

A. Plane wave superposition ray technique

Acoustic guided wave problems are usually formulated in terms of the governing Helmholtz wave equation for displacement. The plane wave superposition technique provides an alternative approach to the solution of guided wave problems without directly solving the governing differential equation. We develop the plane wave superposition technique with reference to the geometry of the equilateral triangle shown in Fig. 2. By using a coordinate transformation through 120° rotation from the (x, y) coordinates on side AB, we introduce the local coordinate systems (x', y') on side BC and (x'', y'') on side AC of triangle ABC assuming origin at the centroid of the triangle as follows:

$$x' = -\frac{1}{2}(x - \sqrt{3}y), \tag{1}$$

$$y' = -\frac{\sqrt{3}}{2}(x + y/\sqrt{3}), \tag{2}$$

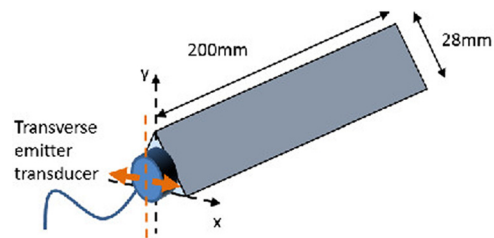


FIG. 1. (Color online) Prismatic waveguide fitted with shear wave transducer.

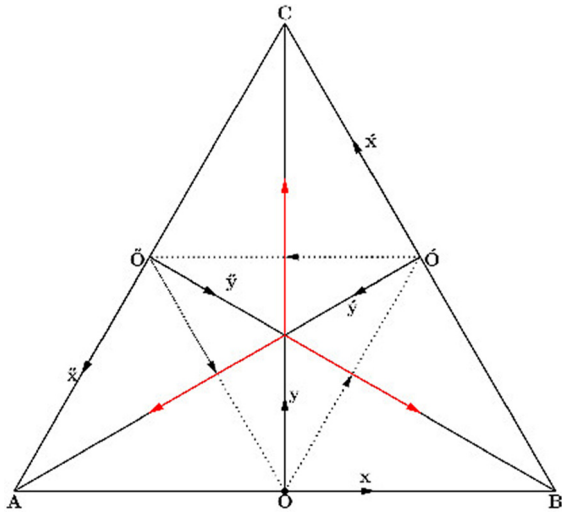


FIG. 2. (Color online) Geometry of equilateral triangle.

$$x'' = -\frac{1}{2}(x + \sqrt{3}y), \tag{3}$$

$$y'' = \frac{\sqrt{3}}{2}(x - y/\sqrt{3}). \tag{4}$$

As well known in waveguide work, a propagating wave having the form $f(x, y)e^{-i\beta z}$ has a cross-sectional mode shape $f(x, y)$ that is completely determined by a superposition of plane waves in the cross section of the guide regardless of whether the wave is propagating or evanescent; i.e., the mode shape is completely determined by waves in the cross section at cutoff. In this case the transverse wavenumber is nothing but the cutoff wavenumber which is an eigenvalue of the transverse Laplacian operator in Helmholtz's equation. In the case of longitudinal wave excitation, each surface of the prismatic guide is acted upon by a set of two-plane waves: one incident and one reflected longitudinal wave set and one incident and one reflected vertically-polarized shear wave set satisfying a condition of transverse resonance producing a partial standing wave field over the surface. Symmetry of the equilateral triangle requires that the same wave picture be present on all three surfaces, so that the total field is obtained by superposition of the three partial wave fields.²⁰ The two sources of the shear-wave transducer model send out waves in opposite directions in order to produce a state of shear. The correct ray picture of the transverse plane waves producing a state of shear is one in which the rays travel parallel to the sides of the triangle. If we trace out the transverse ray path starting from any point of a particular side of the triangle and ending on the same side, the path length traced out by the ray is always a constant equal to $3a/2$ which means the triangle sides are planes of constant phase. This means each side of the triangle is a wavefront and hence can be represented by a plane wave traveling between the midpoints of the sides of the triangle. This is a Δ configuration of rays as seen in Fig. 2. Since two sources are involved, there are two such sets of

rays: one set travels clockwise while the other set is counter-clockwise. This ray picture for a shear wave transducer is used in the ensuing analysis.

Dispersion curves of the guided waves along z direction are easily obtained from a FEM modal analysis (COSMOL® software). The methodology used to compute these dispersion curves is well known.²⁸ A 0.5 mm length triangular waveguide is meshed using 3D tetrahedral elements. The element size l is small enough to ensure convergence of the finite element analysis (mesh refinement does not affect the result) and accurately simulate the wave propagation ($l < \lambda_{min}/10$ with λ_{min} the smaller wavelength along z direction). In order to simulate an infinite extended triangular waveguide, Bloch-Floquet conditions are applied on the two ends of the finite triangular guide.²⁸ This length of the triangular waveguide in the z direction is small enough to remove band folding to the frequency-wavenumber region of interest. Modal analysis of the triangular waveguide shows the existence of dispersion curves of Lamb-like waves (similar to the Lamb waves in a plate) as well as shear-like waves at lower frequencies. In order to distinguish triangular modes from plate modes, we use the Δ symbol to identify the modes of the triangular guide throughout the remainder of the paper. Thus, SH^Δ and SV^Δ designate the triangular SH and SV waves, respectively. As shown in Fig. 3, the first dispersion curve represents the A_0^Δ triangular Lamb wave antisymmetric mode. The second dispersion curve represents the S_0^Δ triangular Lamb wave symmetric mode. These two modes have no cutoff frequency. The S_0^Δ dispersion curve intersects the first SH_1^Δ triangular shear mode dispersion curve whose cutoff wavenumber is $4\pi/(3a)$. This is followed by the A_1^Δ antisymmetric triangular Lamb wave dispersion curve. The first SV_1^Δ vertically polarized shear mode dispersion curve which has cutoff wavenumber $\pi\sqrt{7}/\sqrt{3}a$ intersects the A_1^Δ antisymmetric triangular Lamb wave dispersion curve well above its cutoff frequency of 112 kHz. The second SV_2^Δ vertically polarized shear mode dispersion curve with cutoff wavenumber $2\pi\sqrt{7}/(3a)$ intersects the S_1^Δ triangular Lamb wave dispersion curve near its cutoff frequency at 127 kHz. The SV^Δ shear waves have a nonlinear product solution as explained in Sec. IV.

B. Description of experimental setup

In the experimental setup shown in Fig. 4, an equilateral triangular waveguide of axial length 20 cm made of DURAL AULG aluminum having a side length $a = 28$ mm with shear wave velocity $V_s = 3290$ m/s is placed on three pins so as to avoid coupling from the supporting surface underneath. One triangular face of the sample was fitted with a Panametrics shear wave transducer (1 in. diameter, 500 kHz central frequency). The transducer was driven by a 75 ns duration 200 V amplitude signal having a 200 Hz repetition rate from a Sofranel broadband pulse generator. A Polytec OFV505 laser velocimeter in association with a VD09 digital velocity decoder was used to measure the

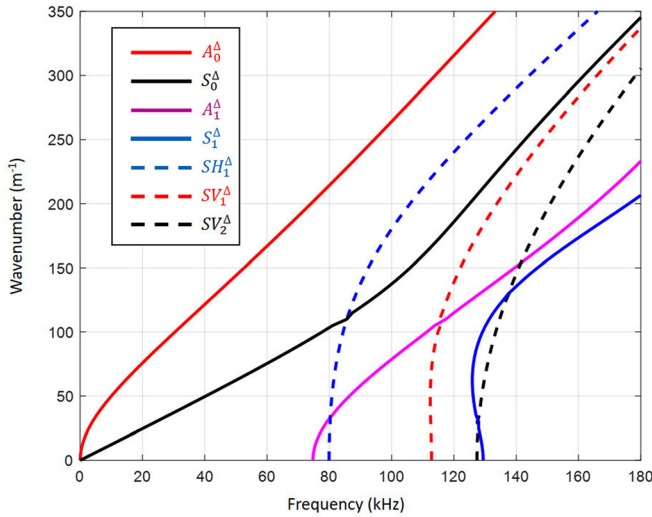


FIG. 3. (Color online) Dispersion curves from COMSOL simulation showing the SH_1^A , SV_1^A , and SV_2^A shear modes.

normal velocity amplitude up to 1.5 MHz. The laser was translated parallel to the guide end face with 0.5 mm space step along the x direction and a 0.866 mm space step along the y direction giving 812 temporal signal acquisitions (Fig. 5). The output of the laser is transmitted to a Le Croy HRO66ZI WaveRunner digital storage oscilloscope. In order to enhance the signal to noise ratio, the registered oscillogram at each position is the mean of 512 successive measurements. As an example, Fig. 6 shows an A-scan signal measured at position $x = 14$ mm and $y = 12.12$ mm near the center of the triangular end surface. The first wave packet seen on this figure extending approximately from 0.15 to 0.4 ms (inside the red dotted box in Fig. 6) corresponds to the waves traveling from the source and guided along the waveguide. The following signals are due to waves that bounced back and forth many times between waveguide ends. The spreading of signals in Fig. 6 is due to the broad frequency range of the excitation. In order to separate and identify the several modes of propagation, a

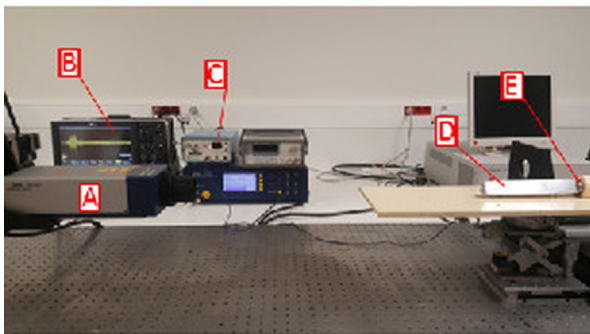


FIG. 4. (Color online) Photograph of the experimental setup including the triangular waveguide (D) on whose back end a Panametrics shear wave transducer (E) is mounted. A Sofranel pulse generator (C) is used to obtain a broadband excitation of the waves in the waveguide. Measurements of the normal surface displacement are performed at the front end of the waveguide with a Polytec laser vibrometer (A) whose output is transmitted to a digital oscilloscope (B) (LeCroy HRO66ZI WaveRunner).

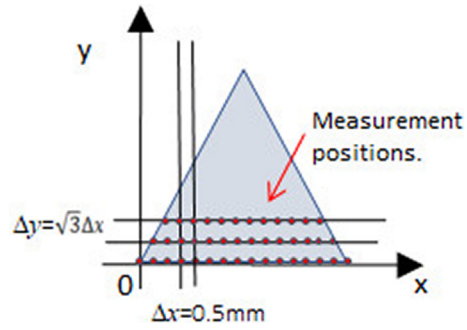


FIG. 5. (Color online) 812 laser measurements are done on the end face of the waveguide with 0.5 mm step along x direction and 0.866 mm step along the y direction.

temporal Fourier transform (FT) is performed on each oscillogram by only selecting the first part of the signal (red box in Fig. 6) so that the reflections on the waveguide ends are not taken into account. The normal displacement over the triangular end is extracted from the FT at each frequency. These experimental modal deformations of the triangular waveguide ends are compared with theoretical normal displacements in the remainder of the paper.

III. CASE OF HORIZONTALLY-POLARIZED-TRIANGULAR SHEAR WAVES

In the equilateral triangular guide, the displacement field of SH^A shear waves is derived from a y -directed vector potential ψ_y giving rise to the two displacement components $u_x = -\partial\psi_y/\partial z$ and $u_z = \partial\psi_y/\partial x$. As was shown in Ref. 20 the x -component is an even function of x while the z -component is an odd function of x . An SH^A wave is by nature not coupled to a longitudinal wave requiring that only tangential displacement components be present over the side surfaces of the guide extending in the z direction. The presence of a normal displacement on any of the side surfaces of the guide changes the wave to the SV^A type which in general couples to a longitudinal wave unless its angle of incidence is 45° in which case it becomes a pure SV^A wave. We first discuss the linear SH^A modes before taking up the analysis of the more involved SV^A modes.

In view of the nature of the shear wave transducer, we determine the SH^A shear wave cross-sectional variation by assuming the existence of two sets of Δ configurations of

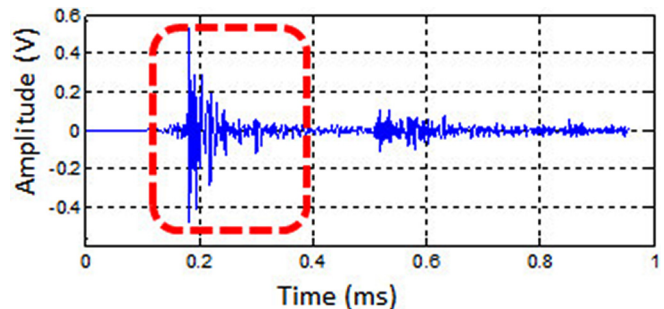


FIG. 6. (Color online) An A-scan signal measured at position $x = 14$ mm and $y = 12.12$ mm in the vicinity of the center of the end surface.

plane waves: a counterclockwise set and a clockwise set 180° out of phase. In solving for the normal displacement, we note that the plane waves of each set do not reverse sign upon reflection as a consequence of the boundary condition on displacement. They rather have an added path phase shift which depends on the transverse wavenumber of the mode. For the mode satisfying the transverse wavenumber $K_s = 4m\pi/(3a)$ with m any integer, we have the following two sequences of plane waves with a path phase shift $2m\pi/3$ responsible for the z -polarized displacement's cross-sectional variation,

$$\begin{aligned} \text{Clockwise } & e^{-iK_s x}, \quad e^{i((K_s/2)(x+\sqrt{3}y)-2m\pi/3)}, \\ & e^{i((K_s/2)(x-\sqrt{3}y)+2m\pi/3)}, \\ \text{Anticlockwise } & -e^{iK_s x}, \quad -e^{-i((K_s/2)(x-\sqrt{3}y)+2m\pi/3)}, \\ & -e^{-i((K_s/2)(x+\sqrt{3}y)-2m\pi/3)}. \end{aligned}$$

We begin the construction of the cross-sectional mode shape $f(x, y)$ of this mode by finding the partial wave fields on the three sides of triangle ABC . Thus, the four waves acting on the surface represented by side AB are $e^{i((K_s/2)(x+\sqrt{3}y)-2m\pi/3)}$, $e^{i((K_s/2)(x-\sqrt{3}y)+2m\pi/3)}$, $-e^{-i((K_s/2)(x+\sqrt{3}y)-2m\pi/3)}$, and $-e^{-i((K_s/2)(x-\sqrt{3}y)+2m\pi/3)}$, which combine to give

$$f(x, y)_{AB} = 4 \sin\left(\frac{K_s x}{2}\right) \cos\left(\frac{\sqrt{3}K_s y}{2} - \frac{2m\pi}{3}\right). \quad (5)$$

On side BC , the four waves acting on the surface are $e^{-iK_s x}$, $e^{i((K_s/2)(x+\sqrt{3}y)-2m\pi/3)}$, $-e^{iK_s x}$, and $-e^{-i((K_s/2)(x+\sqrt{3}y)-2m\pi/3)}$, which combine to give

$$f(x, y)_{BC} = 2 \sin\left(\frac{K_s}{2}(x + \sqrt{3}y) - 2m\pi/3\right) - 2 \sin(K_s x). \quad (6)$$

On side AC , the four waves acting on the surface are $e^{-iK_s x}$, $e^{i((K_s/2)(x-\sqrt{3}y)+2m\pi/3)}$, $-e^{iK_s x}$, and $-e^{-i((K_s/2)(x-\sqrt{3}y)+2m\pi/3)}$, which combine to give

$$f(x, y)_{AC} = 2 \sin\left(\frac{K_s}{2}(x - \sqrt{3}y) + 2m\pi/3\right) - 2 \sin(K_s x). \quad (7)$$

Adding the three partial wave fields from Eqs. (5)–(7) and dividing by 4 (because there are four waves on each surface), we obtain the following normal displacement:

$$u_z = 2 \sin\left(\frac{K_s x}{2}\right) \cos\left(\frac{\sqrt{3}K_s y}{2} - \frac{2m\pi}{3}\right) e^{-i\beta z} - \sin(K_s x) e^{-i\beta z}. \quad (8)$$

This solution satisfies the boundary condition of the vanishing of the normal derivative of u_z on all three surfaces of the waveguide for $m = 1, 2, 3, \dots$. This may be verified by

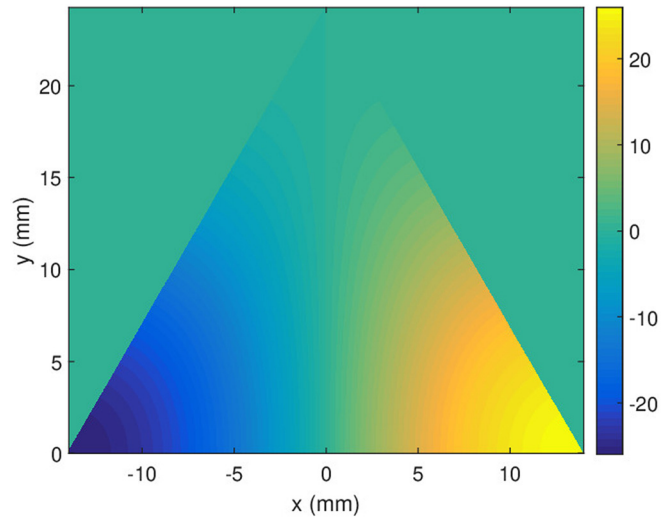


FIG. 7. (Color online) Dimensionless theoretical normal displacement for the triangular SH_1^A ($m=1$) over triangular cross section with cutoff at 78.33 kHz.

transforming coordinates using Eqs. (1)–(4) and taking the derivative with respect to the normal on sides BC and AC . The mode pattern for $m=1$ and $a=28$ mm is shown in Fig. 7 and the corresponding experimental mode shape is shown in Fig. 8. The above plane wave solution is in agreement with the solution of the antisymmetric Neumann problem for displacement.²⁶

We now consider the classical Lamé solution of McCartin²⁵ for the antisymmetric Dirichlet problem satisfied by the shear stress σ_{yz} . These solutions with origin at the midpoint of side AB are characterized by three integers l, m , and n subject to the condition $l + m + n = 0$, and are given by the following cross-sectional mode shape:

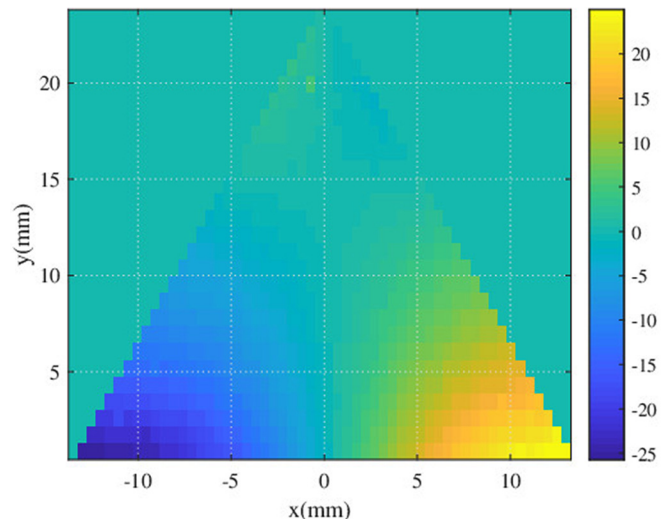


FIG. 8. (Color online) Dimensionless experimental normal displacement for the triangular SH_1^A mode with $m=1$ over triangular cross section measured at 76 kHz.

$$\begin{aligned} \sigma_{yz} = & \sin\left(\pi l - \frac{2\pi ly}{\sqrt{3}a}\right) \sin\left(\frac{2\pi}{3a}(m-n)x\right) \\ & + \sin\left(\pi m - \frac{2\pi my}{\sqrt{3}a}\right) \sin\left(\frac{2\pi}{3a}(n-l)x\right) \\ & + \sin\left(\pi n - \frac{2\pi ny}{\sqrt{3}a}\right) \sin\left(\frac{2\pi}{3a}(l-m)x\right). \end{aligned} \tag{9}$$

Only two of the integers $l, m,$ and n are independent and the cutoff wavenumber (eigenvalue of the transverse Laplacian) is given by

$$K_s^{mn} = \frac{4\pi}{3a} \sqrt{\frac{l^2 + m^2 + n^2}{2}}. \tag{10}$$

The normal displacement u_z is the integral with respect to y of σ_{yz} and is hence given by

$$\begin{aligned} u_z = & \frac{\sqrt{3}a}{2\pi l} \cos(\pi l) \cos\left(\frac{2\pi ly}{\sqrt{3}a}\right) \sin\left(\frac{2(m-n)\pi x}{3a}\right) \\ & + \frac{\sqrt{3}a}{2\pi m} \cos(\pi m) \cos\left(\frac{2\pi my}{\sqrt{3}a}\right) \sin\left(\frac{2(n-l)\pi x}{3a}\right) \\ & + \frac{\sqrt{3}a}{2\pi n} \cos(\pi n) \cos\left(\frac{2\pi ny}{\sqrt{3}a}\right) \sin\left(\frac{2(l-m)\pi x}{3a}\right), \end{aligned} \tag{11}$$

where the propagation factor $e^{-i\beta z}$ is understood and suppressed for brevity.

The normal displacement pattern over the cross section of a bar of side length 28 mm is shown in Fig. 9 for the first mode of Ref. 25 with cutoff frequency at 207.25 kHz and the experimentally measured mode shape shown in Fig. 10 is measured below cutoff at 192 kHz. This is because we are measuring at the bar edge where complex solutions are present and the fact that the bar is short in length enables

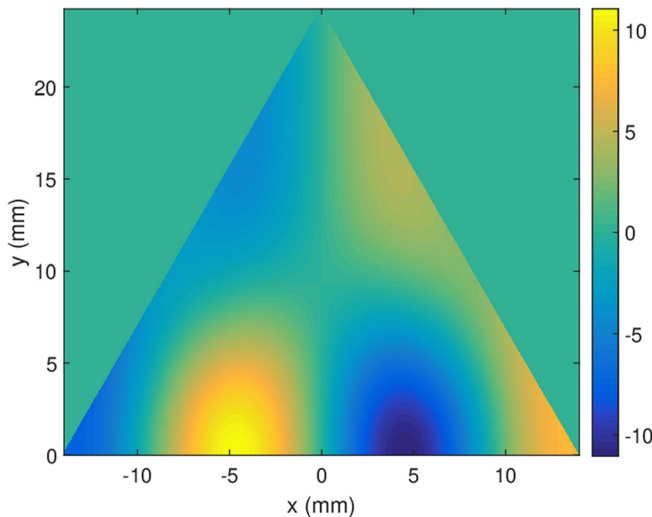


FIG. 9. (Color online) Dimensionless theoretical normal displacement for the first Dirichlet Lamé mode ($m=1, n=2, l=-3$) over triangular cross section with cutoff at 207.25 kHz.

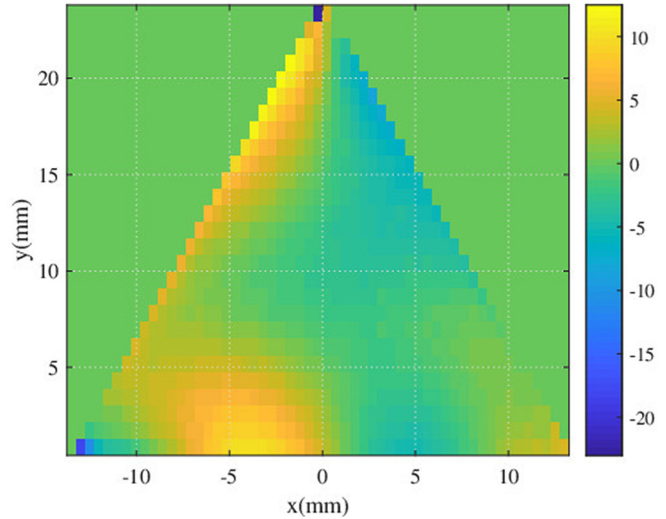


FIG. 10. (Color online) Dimensionless experimental normal displacement for the first Dirichlet Lamé mode ($m=1, n=2, l=-3$) over triangular cross section measured at 192 kHz.

evanescent waves to be measured. The theoretical second Dirichlet Lamé mode shape with cutoff at 282.435 kHz is shown in Fig. 11 and the measured mode shape is shown below cutoff at 244 kHz in Fig. 12. The theoretical third Dirichlet Lamé mode shape with cutoff at 341.447 kHz is shown in Fig. 13 and the measured mode shape below cutoff at 274 kHz is shown in Fig. 14.

IV. CASE OF VERTICALLY POLARIZED-TRIANGULAR SHEAR WAVES

We have already shown that SH waves in the equilateral triangle are obtained from superposition of two sets of three equal plane waves equi-spaced 120° apart and their reflections for the first SH_1^Δ mode. The McCartin solutions²⁵ are likewise obtained from superposition of three standing

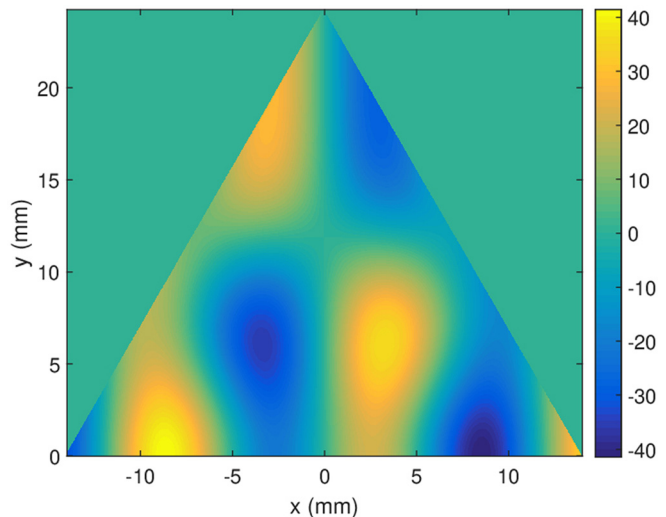


FIG. 11. (Color online) Dimensionless theoretical normal displacement for the second Dirichlet Lamé mode ($m=1, n=3, l=-4$) over triangular cross section with cutoff at 282.435 kHz.

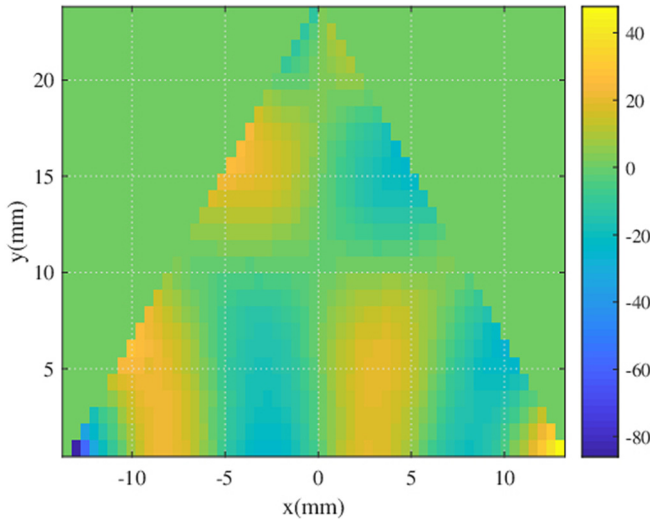


FIG. 12. (Color online) Dimensionless experimental normal displacement for the second Dirichlet Lamé mode ($m=1, n=3, l=-4$) over triangular cross section measured at 244 kHz.

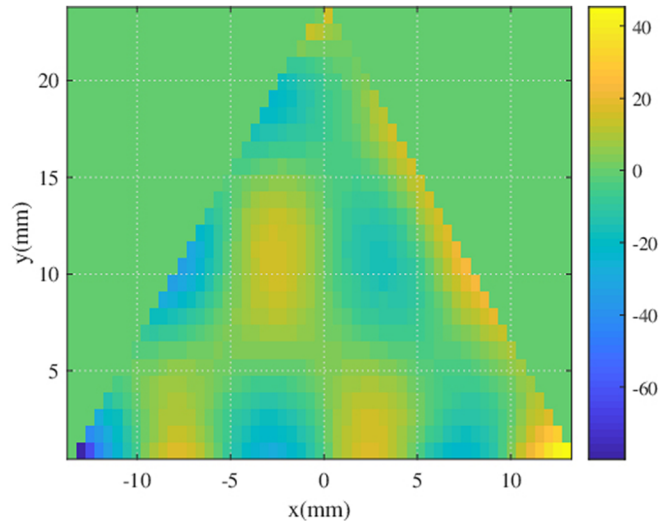


FIG. 14. (Color online) Dimensionless experimental normal displacement for the third Dirichlet Lamé mode ($m=2, n=3, l=-5$) over triangular cross section measured at 274 kHz.

waves. We next examine the standing wave condition in the $30^\circ-60^\circ-90^\circ$ and $30^\circ-120^\circ-30^\circ$ sub triangles and show that they result from three unequal wavenumber vectors that are not equi-angularly spaced and decompose those wavenumber vectors by using the method of symmetrical components^{23,24} into three different sets of three equal vectors each: the first set is a zero sequence set of three equal and parallel vectors that are zero if the original three vectors are balanced, i.e., they add to zero, the second set is a positive sequence set of three equal vectors that are spaced 120° counterclockwise apart, and the third set is a negative sequence set of three equal vectors equi-spaced 120° clockwise apart. For an antisymmetric solution, the equilateral triangle in Fig. 15 is divided in half by the nature of the shear wave transducer. If we assume the right half to have a positive z -displacement, the left half would have a negative

z -displacement with zero displacement on the median CE. Considering the right half triangle of Fig. 15, the simplest standing wave condition is one in which the total phase angle is π in every direction as assumed by Polya.²⁷ Taking the three directions from base to apex, the standing waves in those directions are characterized by three wavenumber phasors $K_1, K_2,$ and K_3 such that $K_1 = \pi/AD = (4\pi/\sqrt{3}a)\angle -150^\circ,$ $K_2 = \pi/AB = (2\pi/a)\angle 0^\circ,$ $K_3 = \pi/AC = (2\pi/\sqrt{3}a)\angle 90^\circ.$ These three unequal phasors are balanced, i.e., they add to zero. Using symmetrical components analysis,^{23,24} we only have the positive sequence of equal phasors K^+ and negative sequence of equal phasors K^- both spaced 120° apart. The transformation to the new system of phasors is effected by the transformation

$$\begin{bmatrix} K_0 \\ K^+ \\ K^- \end{bmatrix} = \frac{1}{3} \begin{bmatrix} 1 & 1 & 1 \\ 1 & \gamma & \gamma^2 \\ 1 & \gamma^2 & \gamma \end{bmatrix} \begin{bmatrix} K_1 \\ K_2 \\ K_3 \end{bmatrix}, \quad (12)$$

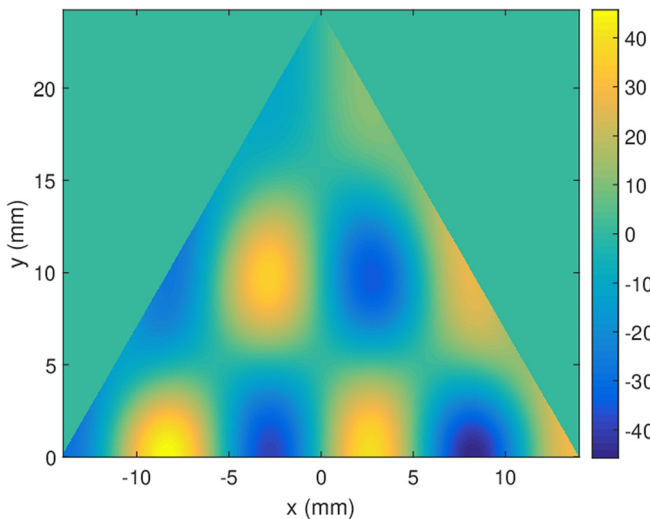


FIG. 13. (Color online) Dimensionless theoretical normal displacement for the third Dirichlet Lamé mode ($m=2, n=3, l=-5$) over triangular cross section with cutoff at 341.447 kHz.

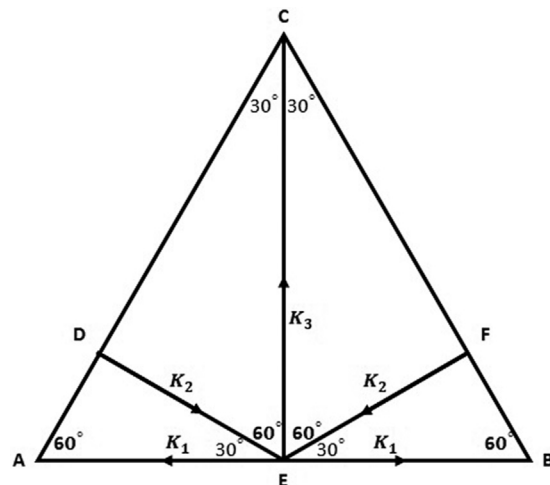


FIG. 15. Standing wave condition in half equilateral triangles.

where $\gamma = e^{2\pi i/3}$. This gives the three positive sequence phasors in the order (red-yellow-blue) $K_R^+ = (2\pi/3a)\angle -180^\circ$, $K_Y^+ = (2\pi/3a)\angle -60^\circ$, $K_B^+ = (2\pi/3a)\angle 60^\circ$. The negative sequence phasors in the order (red-blue-yellow) are given by $K_R^- = (2\pi\sqrt{7}/3a)\angle -139.1^\circ$, $K_B^- = (2\pi\sqrt{7}/3a)\angle -19.1^\circ$, $K_Y^- = (2\pi\sqrt{7}/3a)\angle 100.9^\circ$. In this manner, the phasors of the 30° - 60° - 90° sub triangle are broken down into two sets of equal phasors in the equilateral triangle. In what follows, we show how a product solution based on the positive sequence phasors gives a solution satisfying all three boundary conditions in the equilateral triangle for the SV_1^Δ and SV_2^Δ modes. The negative sequence waveforms are a by-product of the product solution based on the positive sequence.

A. SV wave from bisection of equilateral triangle

We start by presenting the product solution for the half equilateral triangle responsible for the SV_2^Δ wave since the analysis is more straightforward when using the ray technique and develop a general formula for stress that is also satisfied by the SV_1^Δ that comes from trisection of the equilateral triangle. In view of the free surface boundary condition that the shear stress must vanish on the surface, the reflected shear-stress wave must change sign at each reflection. Transverse resonance requires that rays performing a closed circuit from starting point to end point must emerge in phase. Since a ray undergoes three reflections in a Δ configuration, then a total phase shift of 3π radians is involved which requires an additional path phase shift of an odd number of π radians for the rays to emerge in phase. A resonant condition producing an eigenmode is therefore satisfied by a ray traveling between the midpoints of the sides of the triangle with a total path length of $3a/2$ if the transverse wave-number is $K_s = 2m\pi/3a$, with m an odd integer. We begin the formulation by considering the partial wave field of the stress tensor on the surface represented by side AB of the triangle. There are two components of shear stress σ_{xy} and σ_{zy} which have the same y -dependence, and both satisfy a Dirichlet boundary condition at $y = -a/2\sqrt{3}$. For purposes of comparison with experiment, we choose to work with the z - y plane shear stress component σ_{zy} without loss of generality. Since the displacement in the experiment is produced by two transversal transducers, σ_{zy} will be antisymmetric with respect to the y axis on side AB while σ_{xy} will be symmetric. This is based on the assumption that the two transversal transducers are spaced along a line parallel to the x axis. The σ_{zy} shear stress picture over the cross section of the triangle is assumed to be due to the following two sets of three plane waves with normalized amplitudes referred to origin at the centroid:

$$\begin{aligned} \text{Clockwise } & e^{-iK_s x}, \quad e^{i((K_s/2)(x+\sqrt{3}y)+2m\pi/3)}, \\ & e^{i((K_s/2)(x-\sqrt{3}y)-2m\pi/3)}, \end{aligned}$$

$$\begin{aligned} \text{Anticlockwise } & -e^{iK_s x}, \quad -e^{-i((K_s/2)(x-\sqrt{3}y)-2m\pi/3)}, \\ & -e^{-i((K_s/2)(x+\sqrt{3}y)+2m\pi/3)}. \end{aligned}$$

The first set represents the positive sequence of phasors of the left half triangle, while the second set represents the positive sequence of the right half triangle. A propagation factor $e^{i(\omega t - \beta z)}$ is understood and dropped for brevity. Now each surface has four waves acting on it and we can construct the partial fields for each surface. A solution satisfying the boundary condition $\sigma_{zy} = 0$ on side AB is thus given by

$$\sigma_{zy}(AB) = 2 \sin\left(\frac{K_s}{2}x\right) \cos\left(\frac{\sqrt{3}K_s}{2}y + \theta\right), \tag{13}$$

where $\theta = 2m\pi/3$. Similarly, the solution satisfying the boundary conditions $\sigma_{zy'} = 0$ on side BC and $\sigma_{zy''} = 0$ on side AC are given, respectively, by

$$\sigma_{zy'}(BC) = 2 \left(\sin\left[\frac{K_s}{2}(x + \sqrt{3}y) + \theta\right] - \sin(K_s x - 3\theta) \right), \tag{14}$$

$$\sigma_{zy''}(AC) = 2 \left(\sin\left[\frac{K_s}{2}(x - \sqrt{3}y) - \theta\right] - \sin(K_s x + 3\theta) \right). \tag{15}$$

We note here that unlike the case of the triangular SH^Δ waves, a solution by superposition of the three partial fields given by Eqs. (13)–(15) does not satisfy all boundary conditions. For this reason, we take a product of the three partial fields as our solution of the shear wave problem. By expanding the product of Eqs. (13)–(15), we see that the solution may be broken down into three components having transverse wavenumbers K_s , $2K_s$, and $\sqrt{7}K_s$ as follows:

$$\begin{aligned} \sigma_{zy}^1 &= \frac{1}{2} [1 + \cos(6\theta)] \sin\left(\frac{K_s x}{2}\right) \cos\left[\frac{\sqrt{3}K_s}{2}y + \theta\right] \\ &\quad - \frac{1}{2} \sin(K_s x) \cos(3\theta), \end{aligned} \tag{16}$$

$$\begin{aligned} \sigma_{zy}^2 &= -\frac{1}{4} \sin(K_s x) \cos(\sqrt{3}K_s y + 5\theta) \\ &\quad - \frac{1}{4} \sin(K_s x) \cos(\sqrt{3}K_s y - \theta) \\ &\quad + \frac{1}{4} \sin(2K_s x) \cos(3\theta), \end{aligned} \tag{17}$$

$$\begin{aligned} \sigma_{zy}^3 &= \frac{1}{8} \left\{ 2 \sin\left(\frac{K_s}{2}x\right) \cos\left(\frac{3\sqrt{3}K_s}{2}y + 3\theta\right) \right\} \\ &\quad - \frac{1}{8} \left\{ 2 \sin\left(\frac{5K_s}{2}x\right) \cos\left(\frac{\sqrt{3}K_s}{2}y + \theta\right) \right\} \\ &\quad + \frac{1}{8} \left\{ 2 \sin(2K_s x) \cos(\sqrt{3}K_s y + 5\theta) \right\}. \end{aligned} \tag{18}$$

We note that each of the terms inside braces in Eqs. (16)–(18) represents the sum of three partial waves having respectively the cutoff wavenumbers K_s , $2K_s$, and $\sqrt{7}K_s$. In order to find the normal displacement u_z , we note that the same expressions in Eqs. (16)–(18) give the normal

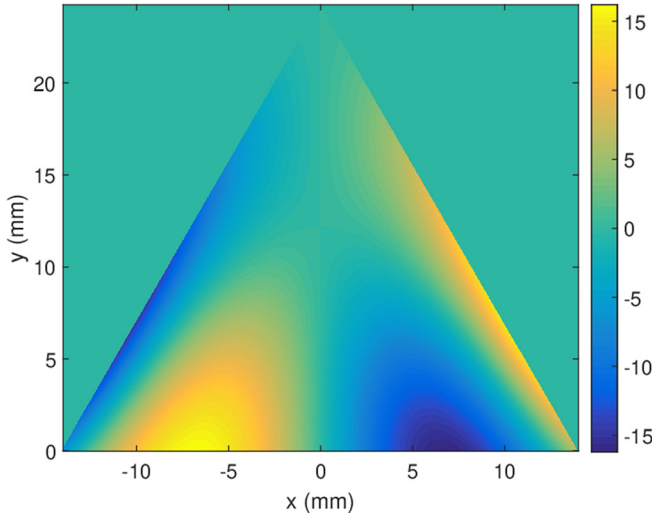


FIG. 16. (Color online) Dimensionless theoretical normal displacement for the SV_1^Δ and SV_2^Δ waves over triangular cross section.

displacement if the cosine functions in y are changed into sine while keeping the same amplitude ratios. Adding the three components of normal displacement, the mode shape of the SV_2^Δ is shown in Fig. 16 and agrees with the experimental mode shape shown in Fig. 17. This mode shape was observed in the experiment to be dominant over a considerable bandwidth from 114 and up to 192 kHz. In order to determine the cutoff frequency of the SV_2^Δ wave, we note that the pure SV^Δ wave occurs when its incident ray is at 45° to the normal of any of the surfaces of the waveguide such that the wavenumber k_s of the incident plane wave is related to the cutoff wavenumber $K_s^{(3)}$ of the third component of the triangular SV_2^Δ wave by

$$K_s^{(3)} = k_s \cos \theta_s / \cos(30^\circ), \quad (19)$$

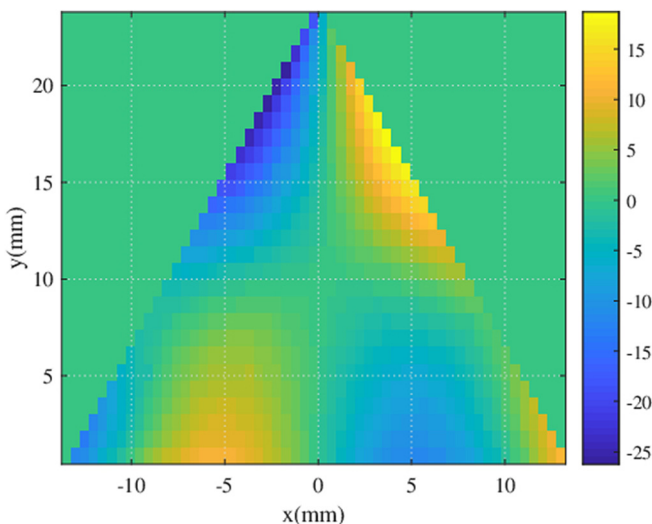


FIG. 17. (Color online) Dimensionless experimental normal displacement for the nonlinear SV_2^Δ wave over triangular cross section at 140 kHz.

where $k_s = \omega/V_s$, θ_s is the angle the incident SV_2^Δ ray makes with the normal to the waveguide surface, and the Δ configuration in the cross section contributes the 30° angle. The SV_2^Δ wave is not fully developed until the third component propagates giving rise to a cutoff frequency

$$f_c = \frac{m\sqrt{7}V_s}{\sqrt{6}a}. \quad (20)$$

For $m = 1$, $V_s = 3290$ m/s, and $a = 28$ mm, this gives a cutoff frequency of 126.9145 kHz in agreement with simulation in COMSOL and experiment.

B. SV wave from trisection of equilateral triangle

If we divide the equilateral triangle into three 30° - 120° - 30° sub triangles as shown in Fig. 18, the standing wave condition can be described by a function satisfying the boundary condition on side AB of triangle in the form $\cos K_1 y$ which vanishes at $y = -a/2\sqrt{3}$ so that $K_1 = \sqrt{3}\pi/a \angle 90^\circ$. Referring to Fig. 18, the phasors perpendicular to the sides of this sub triangle for the same functional dependence are $K_2 = \pi/a \angle -120^\circ$ and $K_3 = \pi/a \angle -60^\circ$. These vectors are also balanced so that symmetrical component analysis only gives a positive sequence set $K_R^+ = \pi/\sqrt{3}a \angle 90^\circ$, $K_Y^+ = \pi/\sqrt{3}a \angle -30^\circ$, $K_B^+ = \pi/\sqrt{3}a \angle -150^\circ$ and a negative sequence set $K_R^- = 2\pi/\sqrt{3}a \angle 90^\circ$, $K_B^- = 2\pi/\sqrt{3}a \angle -30^\circ$, $K_Y^- = 2\pi/\sqrt{3}a \angle -150^\circ$. As we did with the SV_2^Δ wave, we attempt a product solution based on the positive sequence of plane waves with wavenumber $K_s = \pi/\sqrt{3}a$ and change the phase shift in Eqs. (13)–(15) from $2\pi/3$ to $\theta = \pi/2 + \pi/(4\sqrt{3})$. The theoretically calculated normal displacement is the same pattern as that of the SV_2^Δ mode shown in Fig. 16 but at a cutoff frequency of 109.9 kHz in good agreement with simulation. The corresponding experimentally measured normal displacement is shown in Fig. 19 at 116 kHz.

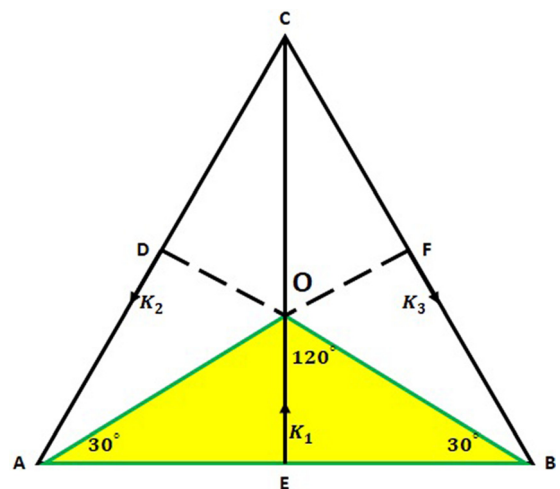


FIG. 18. (Color online) Standing wave condition in 30° - 120° - 30° sub triangle.

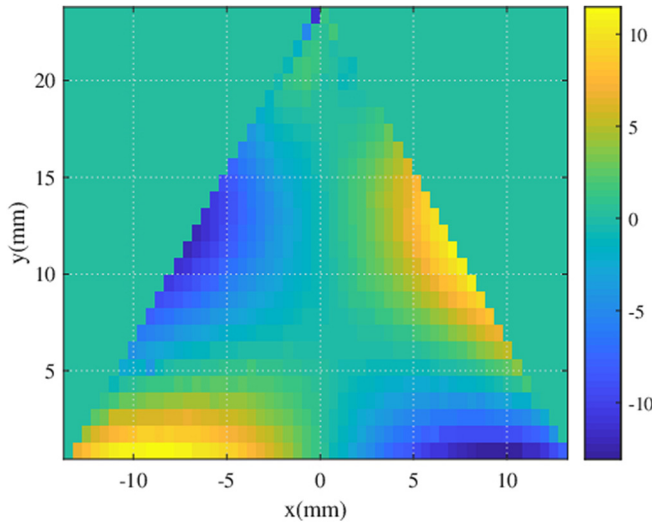


FIG. 19. (Color online) Dimensionless experimental normal displacement for the triangular SV_1^Δ mode over triangular cross section measured at 116 kHz.

V. CONCLUSIONS

In this paper we proposed and used a plane wave reconstruction technique to find exact solutions that satisfied all stress-free boundary conditions in a prismatic waveguide of equilateral triangular cross section for horizontally polarized and vertically polarized shear waves. It was found that cut-off frequencies were in good agreement with their corresponding values found in the experiment as was also confirmed by simulation in COMSOL that was used to calculate the dispersion curves shown in Fig. 3. The normal displacement shapes of the SH^Δ and SV^Δ modes as well as the modes of the classical Lamé solution^{25,26} were confirmed experimentally. However, the measured mode shapes in the experiment were observed below their theoretical cutoffs as evanescent modes which were possible to observe due to the fact that the waveguide specimen was short in length compared to the wavelength near cutoff. The normal displacement mode shape of the SV_2^Δ wave in the experiment shown in Fig. 17 agrees with the theoretical mode shape shown in Fig. 16. Also, the measured normal displacement mode shape of the SV_1^Δ mode shown in Fig. 19 is in good agreement with the theoretical mode shape shown in Fig. 16. This mode shape seems to be dominant over a wide frequency range in the experiment and is also similar to the mode shape of the first Dirichlet classical Lamé solution²⁵ occurring at a higher frequency. Moreover, these two modes have essentially the same stress pattern over the cross section of the bar as shown in Fig. 20 despite the fact that cutoff wavenumbers of the SV_2^Δ and the first Dirichlet Lamé mode are in the ratio 1 : 2.

This study revealed that SH^Δ waves are obtained from superposition of three equal plane waves and their reflections in an equilateral triangle and that SV^Δ waves are obtained from a nonlinear product solution based on symmetrical components analysis of the simplest standing wave conditions in the $30^\circ\text{--}60^\circ\text{--}90^\circ$ and $30^\circ\text{--}120^\circ\text{--}30^\circ$ sub

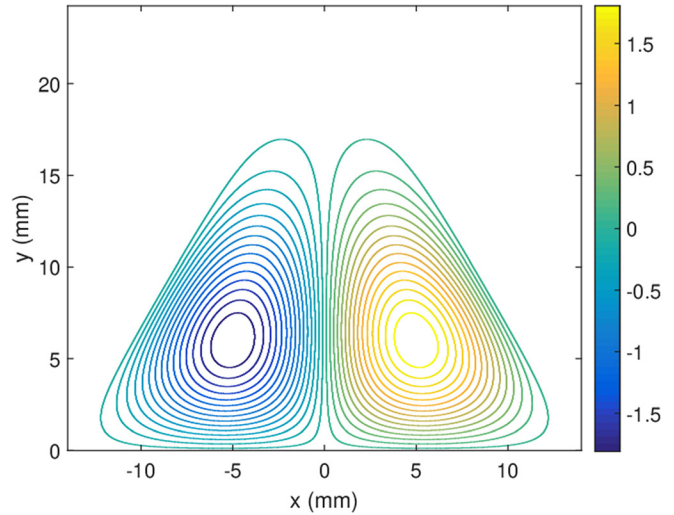


FIG. 20. (Color online) Dimensionless theoretical stress contours of SV^Δ waves and first Lamé solution over triangular cross section.

triangles within the equilateral triangle. Identification of the modes of a waveguide structure is a first step towards more involved studies of mode coupling in complex structures such as a V-weld in a plate. In this case the V-weld will have one stress-free boundary condition. The other two continuity boundary conditions along the two sides of the weld will be those of a surface wave which attenuates spatially in the adjoining metal. This will be the subject of future theoretical and experimental research.

¹S. David, S. Babu, and J. Vitek, “Welding: Solidification and micro-structure,” TMS ONLINE, <https://www.tms.org/pubs/journals/JOM/0306/David-0306.html> (Last viewed October 21, 2018).
²A. Paradowska, J. W. H. Price, R. Ibrahim, and T. Finlayson, “A neutron diffraction study of residual stress due to welding,” *J. Mater. Process. Technol.* **164–165**, 1099–1105 (2005).
³D. Marcuse, *Light Transmission Optics* (Van Nostrand Reinhold, New York, 1972).
⁴Z. Fan, “Application of guided wave propagation on waveguides with irregular cross-section,” Ph.D. thesis, Imperial College, London (2010).
⁵Z. Fan and M. Lowe, “Elastic waves guided by a welded joint in a plate,” *Proc. R. Soc. A: Math. Phys. Eng. Sci.* **465**, 2053–2068 (2009).
⁶C. Chree, “Longitudinal vibrations of a circular bar,” *Q. J. Pure Appl. Math.* **21**, 287–298 (1886).
⁷P. Wong, J. Miklowitz, and R. Scott, “Propagation of harmonic flexural waves in an infinite elastic rod of elliptical cross section,” *J. Acoust. Soc. Am.* **40**, 393–398 (1966).
⁸N. Nigro, “Steady-state wave propagation in infinite bars of noncircular cross section,” *J. Acoust. Soc. Am.* **40**, 1501–1508 (1966).
⁹K. Nagaya, “Dispersion of elastic waves in bars with polygonal cross sections,” *J. Acoust. Soc. Am.* **70**, 763–770 (1981).
¹⁰O. Mukdadi, Y. Desai, S. Datta, A. Shah, and A. Niklasson, “Elastic guided waves in a layered plate with rectangular cross section,” *J. Acoust. Soc. Am.* **112**, 1766–1779 (2002).
¹¹B. Mace, D. Duhamel, M. Brennan, and L. Hinke, “Finite element prediction of wave motion in structural waveguides,” *J. Acoust. Soc. Am.* **117**, 2835–2843 (2005).
¹²M. Predoi, M. Castaings, B. Hosten, and C. Bacon, “Wave propagation along transversely periodic structures,” *J. Acoust. Soc. Am.* **121**, 1935–1944 (2007).

- ¹³M. Predoi, M. El Kettani, Z. Hamitouche, and C. Petre, "Guided waves in plates with linear variation in thickness," *J. Acoust. Soc. Am.* **123**, 3834 (2008).
- ¹⁴M. Castaings and M. Lowe, "Finite-element model for waves guided along solid systems of arbitrary section coupled to infinite media," *J. Acoust. Soc. Am.* **123**, 696–708 (2008).
- ¹⁵F. Cegla, "Energy concentration at the center of large aspect ratio rectangular waveguides at high frequencies," *J. Acoust. Soc. Am.* **123**, 4218–4226 (2008).
- ¹⁶J. Lesage, J. Bond, and A. Sinclair, "Elastic wave propagation in bars of arbitrary cross section: A generalized Fourier expansion collocation method," *J. Acoust. Soc. Am.* **136**, 985–992 (2014).
- ¹⁷V. Krylov, "Conditions for validity of the geometrical acoustics approximation in application to waves in an acute-angle solid wedge," *Sov. Phys. Acoust.* **35**, 176–180 (1989).
- ¹⁸J. W. S. Rayleigh, *Theory of Sound*, 2nd ed. (Dover Publications, New York, 1945), the triangle is discussed in Sec. 199.
- ¹⁹G. Hudson, "Dispersion of elastic waves in solid circular cylinders," *Phys. Rev.* **63**, 46–51 (1943).
- ²⁰O. Asfar and B. Morvan, "Vibrational modes of equilateral triangular solid bars," in *Proceedings of the 2016 IEEE International Ultrasonics Symposium*, Tours, France (September 18–21, 2016).
- ²¹J. Wang, Q. Liu, and L. Zhu, "Bandwidth enhancement of a differentially-fed equilateral triangular patch antenna via loading of shorting posts," *IEEE Trans. Ant. Propagat.* **65**, 36–43 (2017).
- ²²G. Lamé, *Leçons Sur la Théorie Mathématique de L'Elasticité Des Corps Solides*, Deuxieme ed. (*Lessons on the Mathematical Theory of the Elasticity of Bodies Solids*, 2nd ed.) (Cauthier-Villars, Paris, 1866).
- ²³C. L. Fortescue, "Method of symmetrical coordinates applied to the solution of polyphase networks," in *Transactions of the American Institute of Electrical Engineers* (1918), Vol. XXXVII, No. 2, pp. 1027–1140.
- ²⁴B. M. Weedy, *Electric Power Systems* (John Wiley and Sons, New York, 1979), pp. 253–256.
- ²⁵B. McCartin, "Eigenstructure of the equilateral triangle, Part I: The Dirichlet problem," *SIAM Rev.* **45**, 267–287 (2003).
- ²⁶B. McCartin, "Eigenstructure of the equilateral triangle, Part II: The Neumann problem," *Math. Probl. Eng.* **8**, 517–539 (2002).
- ²⁷G. Polya, "A note on the principal frequency of a triangular membrane," *Q. Appl. Math.* **8**, 386 (1951).
- ²⁸C. Hakoda, J. Rose, P. Shokouhi, and C. Lissenden, "Using Floquet periodicity to easily calculate dispersion curves and wave structures of homogeneous waveguides," *AIP Conf. Proc.* **1949**, 020016 (2018).